

The use of quantitative imaging to investigate regulators of membrane trafficking in Arabidopsis stomatal closure

Gildas Bourdais^{1*}, Deirdre H. McLachlan^{1,2*}, Lydia M. Rickett^{1*}, Ji Zhou^{1,3*}, Agnieszka Siwoszek¹, Heidrun Häweker¹, Matthew Hartley⁴, Hannah Kuhn^{1,5}, Richard J. Morris⁴, Dan MacLean¹, and Silke Robatzek¹

¹The Sainsbury Laboratory, Norwich Research Park, Norwich, NR4 7UH, UK.

²School of Biological Sciences, University of Bristol, 24 Tyndall Ave, Bristol, BS8 1TQ.

³The Earlham Institute, Norwich Research Park, Norwich, NR4 7UH, UK.

⁴John Innes Centre, Norwich Research Park, Norwich, NR4 7UH, UK.

⁵Unit of Plant Molecular Cell Biology, Institute for Biology I, RWTH Aachen University, Worringerweg 1, 52056 Aachen, Germany.

*These authors contributed equally.

This article has been accepted for publication and undergone full peer review but has not been through the copyediting, typesetting, pagination and proofreading process which may lead to differences between this version and the Version of Record. Please cite this article as doi: 10.1111/tra.12625

Author contributions:

G.B., D.H.M., A.S., H.H., H.K., D.M. and S.R. designed research; G.B., D.H.M., J.Z., A.S., H.H. and D.M. performed research; G.B., D.H.M., L.R., J.Z. A.S., H.H., M.H., H.K., D.M., R.J.M. and S.R. analysed data; D.H.M., L.R. and S.R. wrote the paper with inputs from all authors.

Corresponding author: Silke Robatzek, The Sainsbury Laboratory, Tel.: +44-1603-450-408, Email: robatzek@tsl.ac.uk

Keywords: Immunity, flg22, FLS2, chitin, ABA, ROS, calcium, endosome, ARA6, ARA7

Running title: Trafficking-mediated stomatal immunity

Manuscript information: Abstract (168 words), total character count 38,044 (excluding references); 82 references

The number of figures: 4 main figures; 10 supplemental figures; 2 supplemental tables

Synopsis

High-throughput imaging at cellular and subcellular scales enables genetic dissection of plant physiological responses to biotic and abiotic stresses. We developed the software tool StomataMeasurer allowing the identification and measurements of stomatal apertures in an automated fashion. Using *Arabidopsis* mutant screening, we demonstrate that StomataMeasurer is suitable to analyze stomatal patterning and behaviors in response to five stimuli.

Abstract

Expansion of gene families facilitates robustness and evolvability of biological processes but impedes functional genetic dissection of signalling pathways. To address this, quantitative analysis of single cell responses can help characterise the redundancy within gene families. We developed high-throughput quantitative imaging of stomatal closure, a response of plant guard cells, and performed a reverse genetic screen in a group of *Arabidopsis* mutants to five stimuli. Focussing on the intersection between guard cell signalling and the endomembrane system, we identified eight clusters based on the mutant stomatal responses. Mutants generally affected in stomatal closure were mostly in genes encoding *SNARE* and *SCAMP* membrane regulators. By contrast, mutants in *RAB5 GTPase* genes played specific roles in stomatal closure to microbial but not drought stress. Together with timed quantitative imaging of endosomes revealing sequential patterns in FLS2 trafficking, our imaging pipeline can resolve non-redundant functions of the RAB5 GTPase gene family. Finally, we provide a valuable image-based tool to dissect guard cell responses and outline a genetic framework of stomatal closure.

Introduction

Signal transduction is initialized to specific stimuli and induces a series of molecular events that regulate cellular responses. Distinct signal transduction pathways can interact with each other to form signalling networks and allow the coordinated cellular response to different developmental and environmental cues^{1 2 3}. Thus, dissecting signalling pathways is important for understanding biological processes. For many biological processes, the signalling pathways have been revealed through forward and reverse genetic screening, which typically involves the manual inspection of mutant phenotypes from large populations^{4 5 6}. However, a large number of molecular components governing signal transduction are yet to be discovered and often remain elusive due to lethality and redundancy issues of gene families^{7 8}. To overcome the complexity of whole plant/organ systems with different cell types, single cell models are increasingly used to dissect signalling pathways in combination with quantitative high-throughput screening systems^{9 10 11 12}.

In plants, guard cells are ultimately isolated from the symplast and therefore have been well established as a single cell model system^{13 14 15}. A pair of guard cells forms the stomatal pore evolved to facilitate photosynthetic gas exchange and water transpiration across the leaf epidermal barrier¹⁶. Proper pore adjustment results in plant adaptation to environmental stresses¹⁶. For example, drought stress is signalled by increased levels of abscisic acid (ABA), which induces the closure of stomata and thus limits water loss. Being pores, many potentially infectious pathogens seek open stomata for invading leaf tissues^{17 18 19}. To limit the entry of pathogens, guard cells detect microbe-associated molecular patterns (MAMPs) by plasma membrane (PM)-localized pattern recognition receptors (PRRs) and trigger closure of stomata^{16 17 20}. Thus, as stomatal apertures are controlled in response to environmental signals, guard cells have been successfully used to dissect signalling pathways including abscisic acid (ABA)- and immune signal transduction^{16 21 22}.

Both ABA- and MAMP-induced stomatal closure requires activation of S-type anion channels mediated by the SLOW ANION CHANNEL-ASSOCIATED 1 (SLAC1), a weak rectifying anion channel present at the plasma membrane of guard cells, and closely related SLAC1

HOMOLOG 3 (SLAH3)²³. SLAC1 is activated by OPEN STOMATA 1 (OST1), a SUCROSE NON-FERMENTING 1 (SNF1)-related protein kinase (SnRK), and members of the CALCIUM-DEPENDENT PROTEIN KINASE (CPK) family as well as CALCINEURIN B-LIKE (CBL) and CBL-INTERACTING PROTEIN KINASE (CIPK) family members^{24 25 26 27 28}. By contrast, SLAH3 is only activated upon co-expression of CPKs and CBL/CIPKs but not by OST1^{28 29}. This demonstrates that different kinases from distinct families regulate the activity of S-type anion channels. Stomatal closure induced by the bacterial MAMP flagellin, which is perceived by the FLAGELLIN SENSING 2 (FLS2) receptor through the elicitor active epitope flg22²⁰, also seems to involve OST1^{19 30 31}. The finding that OST1 and SLAC1/SLAH3 mediate closure of stomata induced by many biotic and abiotic stimuli suggests convergence of the guard cell signalling pathways that close stomata¹⁶.

Proper signal transduction depends on the intersection with the endomembrane system³². Links between guard cell signalling and membrane trafficking are necessary for regulation of the 30-40% guard cell surface area changes during stomatal opening and closure^{16 33}. Unexpectedly, regulators of membrane and protein trafficking such as CLATHRIN HEAVY CHAIN 2 (CHC2) and components of the ENDOSOMAL COMPLEX REQUIRED FOR TRANSPORT-I (ESCRT-I) appear to be specifically required for closure induced by flg22 but not ABA^{34 35}. Of note, both CHC2 and ESCRT-I mediate endocytosis of ligand-activated FLS2^{34 35}. However, the relationship between these processes is not well understood. Quantitative high-throughput screening is a powerful approach to dissect membrane trafficking, and being quantitative and at single cell (or subcellular) resolution, overcoming lethality and redundancy issues^{12 35 36}. We present a quantitative image-based screen in *Arabidopsis thaliana* to identify components of the endomembrane system involved in guard cell responses to five stimuli. Focussing our attention on RAB5 GTPases, a small gene family in *A. thaliana*³⁷, we tested mutants in the conventional *RAB5 GTPases* *ARABIDOPSIS THALIANA RAB 7 (ARA7)* and homologous *RAB HOMOLOG 1 (RHA1)* as well as the plant-unique RAB5 GTPase *ARA6* in restricting bacterial invasion as well as their effect on FLS2 endocytosis. Our image-based screen provides a valuable tool to dissect the

intersection of guard cell signalling with the endomembrane system and outlines a genetic framework of stomatal closure.

Results

Quantitative imaging of stomatal closure

Light microscopy is a powerful tool to investigate stomatal behaviours^{15 16}. Combined with quantitative image and data analysis, it has vastly expanded the potential for genetic screening^{9 38}. To automate measurements of stomatal pores, we used an image analysis framework for high-content screening and developed the StomataMeasurer tool that performs both stomatal pore object detection combined with quantification. For stomatal pore detection, we imaged autofluorescence signals present at the stomatal lip followed by detection of the inner pore (Figure 1). StomataMeasurer produced accurate measurements of stomatal pores in *Arabidopsis* cotyledons allowing for quantification of stomatal behaviours (Figure S1).

To assess the utility of StomataMeasurer for genetic screening, we tested this image object detection tool on stomatal patterns in *Arabidopsis* cotyledons across a collection of mutants in genes including *TOO MANY MOUTHS (TMM)* and *STOMATAL DENSITY AND DISTRIBUTION 1 (SDD1)*, known regulators of stomatal density and distribution (Table S1)^{39 40}. StomataMeasurer was able to detect aberrant stomatal patterns (Figure S2). Measurements of the stomatal pore length and distance between stomata confirmed previously described phenotypes of *tmm* and *sdd1-1* mutants in stomatal development. In addition, we identified that mutants in the *TWO-PORE K⁺ CHANNEL 1 (TPK1)* exhibited shorter stomatal pore length compared to wild type plants (Figure S2). TPK1 encodes a vacuolar membrane localized K⁺ channel that controls cytoplasmic potassium homeostasis⁴¹, which also appears important for determining stomatal pore length.

We then tested the application of StomataMeasurer on stomatal closure. For this analysis, we incubated *Arabidopsis* cotyledons with flg22 and ABA with increasing time. StomataMeasurer pore detection identified decreased stomatal apertures with increasing

concentrations and time of treatments (Figure S3). Taken together, these data suggest that StomataMeasurer could be exploited for analysing stomatal parameters suited for genetic screening.

Stomatal closure induced by flagellin

We applied high-throughput confocal imaging integrating computational image analysis to profile altered stomatal closure in flg22-treated Arabidopsis cotyledons across a collection of mutants in genes known to function in membrane trafficking, with the aim of gaining insights into the potential link between guard cell signalling and the endomembrane system (Table S1). Our collection was based on homozygous T-DNA insertion lines, not excluding the possibility of unaffected and partially affected production of transcripts, and also included mutants in immune signalling to validate our method. We first examined known mutants in FLS2 signalling including the *fls2* receptor and *rbohD* mutants^{16 20}. Images processed with StomataMeasurer confirmed that upon flg22 treatment stomatal pores remained more open in *fls2* and *rbohD* mutants compared to wild type plants (Figure 2, Figure S4). Consistent with MITOGEN-ACTIVATED KINASE 3 (MPK3) activation by FLS2 signalling²⁰, *mpk3* mutants were impaired in flg22-induced stomatal closure^{31 42}. These results demonstrate that StomataMeasurer enables the identification of altered stomatal closure patterns suited for mutant screening.

A total of 54 mutants were screened for altered flg22-induced stomatal closure by confocal imaging combined with StomataMeasurer analysis. In the context of our bias mutant selection, the stomata of 44 mutants did not show significant closure indicating their involvement in FLS2 guard cell signalling and confirming bias in our selected group of *A. thaliana* mutants (Figure 2, Figure S4). For example, *high leaf temperature 1 (ht1)* mutants did not close stomata in response to flg22 (Figure 2, Figure S4). *HT1* codes for a Raf-like kinase and functions as a negative regulator of closure by inhibiting SLAC1⁴³. This could suggest a role for HT1 in SLAC1-mediated stomatal closure to flg22^{19 30 31}. Notably, 21 mutants in genes related to membrane trafficking were affected in flg22-induced stomatal closure. For example, stomatal closure to flg22 was impaired by genetic mutation of

components of SOLUBLE NSF ATTACHMENT PROTEIN RECEPTOR (SNARE) complexes, which included VESICLE-ASSOCIATED MEMBRANE PROTEINs (VAMPs) 721 and 722, VESICLE TRANSPORT THROUGH T-SNARE INTERACTION 11 (VTI11) and VTI12. SNAREs are key components of the membrane trafficking machinery facilitating the fusion of vesicles to target membranes⁴⁴. Thus, together with the role of the SYNAPTIC FUSION 11 (SYN11) SNARE in the regulation of K⁺ channel traffic affecting stomatal pore control⁴⁵, our findings highlight the involvement of SNAREs in the intersection between guard cell signalling and the endomembrane system.

We also found that *ara7*, *rha1* and *ara6* mutants were all altered in stomatal closure induced by *flg22* (Figure 2, Figure S4). ARA7, RHA1 and ARA6 encode homologous RAB5 GTPases in *A. thaliana*³⁷, yet our findings suggest separate functions of them in stomatal immunity. Consistently, although they all localize to endocytic compartments, the RAB5 GTPases only exhibit partially overlapping patterns, i.e. ARA6 preferentially residing on late endosomes^{46 47 48}. Of note, RHA1 is highly expressed in guard cells⁴⁹. As RAB GTPases regulate the fusion of vesicles with target membranes³⁷, our findings further highlight a role for vesicle trafficking in *flg22*-induced guard cell signalling. These results show that quantitative high-throughput imaging of single cell responses represents a valuable tool to dissect the involvement of gene family members in signal transduction events.

ABA-induced stomatal closure

Given the partial convergence of *flg22*- and ABA-induced guard cell signalling pathways that close stomata¹⁶, we next profiled stomatal closure in ABA-treated Arabidopsis cotyledons of the mutants. The stomata of 20 mutants did not significantly close in response to ABA (Figure 2, Figure S5). Unexpectedly, *bak1* and *pub12/13* closed stomata to ABA, which is in disagreement with previous reports^{50 51}. For *pub12/13* mutants, this might be explained by their relatively weak stomatal phenotype⁵¹. A total of 9 mutants related to membrane trafficking were altered in ABA-induced stomatal closure (Figure 2, Figure S5). Of these, all *scamp* mutants, *vti11*, and *rha1* failed to close stomata in response to both ABA and *flg22* (Figure 2, Figure S4 and Figure S5) suggesting that they are more generally impaired in the

intersection between the endomembrane system and guard cell signalling. By contrast, stomata of *vamp721*, *vamp722*, *vti12*, *vti13*, *ara7* and *ara6* mutants, which remained significantly more open upon flg22 trigger (Figure 2, Figure S4), did close in response to ABA (Figure 2, Figure S5). These results suggest that SNAREs and RAB5 GTPases exhibit overlapping and distinct roles in ABA- and flg22-induced stomatal closure.

Chitin-induced stomatal closure

General stomatal responses to pathogens are conserved across kingdoms. Bacterial EF-Tu, lipopolysaccharide and fungal chitin all inhibit opening and promote closure of stomata^{19 52}. To address whether stomatal closure by different MAMPs requires similar molecular components, we determined the stomatal closure in Arabidopsis cotyledons of 42 mutants treated with chitin, a fungal MAMP²⁰. We found that chitin treatment did not significantly close the stomata of 32 mutants (Figure 2, Figure S6). These did not include the *fls2* receptor mutant or *bik1*. In agreement with the latter, immune signalling induced by chitin is predominantly mediated by PBL27⁵³. Unexpectedly, we found that *bak1* mutants were also impaired in chitin-induced stomatal closure (Figure 2, Figure S6). Furthermore, all tested *snare* and *scamp* mutants, except *scamp5*, were affected in chitin-induced stomatal closure (Figure 2, Figure S6), which was shared with stomatal closure by flg22 but not with ABA (Figure 2, Figure S4 and Figure S5). By contrast, of the *rab5* GTPase mutants, *ara7* and *rha1* but not *ara6* showed significantly impaired stomatal closure in response to chitin (Figure 2, Figure S6), while all did not significantly close stomata to flg22, and *rha1* was also affected in ABA-induced stomatal closure (Figure 2, Figure S4 and Figure S5). Our data thus suggest that several membrane trafficking components are shared in MAMP guard cell responses, despite perception by distinct PRR complexes, and that the requirement of RAB5 GTPases in stomatal closure differed between stimuli.

Stomatal closure induced by second messengers

Since impaired stomatal closure upon biotic stimuli could also be caused by a deficiency in guard cell generation of second messengers, we next tested the ability of 48 and 50 mutants to close stomata in response to Ca²⁺ (CaCl₂) and ROS (H₂O₂) respectively, both of which are

Accepted Article

elevated upon flg22 trigger^{16 20}. Stomatal closure by Ca²⁺ was significantly affected in 30 mutants (Figure 2, Figure S7), while closure by H₂O₂ was impaired in 37 mutants (Figure 2, Figure S8), and stomata of 29 mutants did not significantly close by both stimuli (Figure 2, Figure S7 and Figure S8). As expected, these did not include the *rbohD* mutant involved in the converged guard cell signalling pathway¹⁶, as their stomata closed in response to CaCl₂ and H₂O₂ treatments, agreeing with their known role upstream of both second messengers¹⁶. The stomata of all tested mutants of *SNARE* and *SCAMP* trafficking regulators, except *scamp5*, did not close in response to both CaCl₂ and H₂O₂ treatments (Figure 2, Figure S7 and Figure S8). This suggests that although members of multigene families, there is little functional redundancy within the tested *SNARE* and *SCAMP* genes in the stomatal closure response acting downstream of second messengers. Of the *rab5* GTPase mutants, *rha1* and *ara6* did not show significant stomatal closure to H₂O₂ while all closed significantly upon CaCl₂ treatment. This could suggest RAB5 GTPase-mediated trafficking functioning downstream of ROS perception.

We further compared all measurements of stomatal closure to examine whether any of the mutants were specifically affected in MAMP-induced stomatal closure. Nine mutants were impaired in stomatal closure by all tested stimuli (Figure 2). These mutants that are generally defective in stomatal closure were not impaired in stomatal development, excluding the possibility of pleiotropic phenotypes (Figure S9). Thus, the genes affected in these mutants could represent components of the core guard cell signalling pathway underlying stomatal closure. Five are mutants in genes coding for SNARE components highlighting the importance of the intersection between membrane trafficking and signal transduction in the regulation of stomatal aperture. By contrast, *ara7* was found to be specific to MAMP-induced stomatal closure (Figure 2), suggesting a specific role in MAMP-induced stomatal regulation that is shared between flg22 and chitin.

Furthermore, we identified eight significant clusters based on their stomatal response (Figure 2). Cluster 8 represents mutants impaired in stomatal responses to most stimuli, which contains many mutants coding for genes in membrane trafficking. Cluster 6 predominantly

groups mutants impaired in flg22-induced stomatal closure. Consequently, this cluster contains most mutants coding for genes in the FLS2 pathway. Most mutants not or slightly impaired in ABA- and flg22-induced stomatal closure group into cluster 4 and 5, whereas most mutants specifically not or slightly affected in stomatal closure to ABA group into cluster 1 to 3. Interestingly, we found *rha1* mutants in cluster 6, suggesting its predominant role is in the FLS2 pathway. Comparing all *rab5* GTPase mutants, despite being impaired in flg22-induced stomatal closure, they group into different clusters, which suggests distinct but overlapping functions in the regulation of stomatal immunity by these homologous RAB5 GTPases.

RAB5 GTPases mediate stomatal immunity

To gain insights into the role of the RAB5 GTPases in stomatal immunity⁵⁴ as identified from our screen, we tested the mutants for FLS2-mediated immune responses. Since impaired stomatal closure in response to MAMPs could cause an increase in susceptibility to bacterial infection, we next examined the *rha1*, *ara7* and *ara6* mutants, also including the *ara6 x ara7* double mutant, for impaired anti-bacterial immunity. We first infected plants by surface-inoculating wild type *Pseudomonas syringae* pv. *tomato* (*Pto*) DC3000 coronatine-deficient (*cor-*) bacteria that fail to enter through closed stomata¹⁹. All mutants showed elevated bacterial growth as compared to wild type plants (Figure 3A). We then infected the mutants by leaf-injecting *Pto* DC3000 *cor-* bacteria and found no difference in anti-bacterial immunity between wild type plants and the *rha1*, *ara7*, *ara6* and *ara6 x ara7* mutants (Figure 3B). These results are in agreement with their impaired flg22-induced stomatal closure (Figures 2, Figure S4) and suggest a non-redundant function of the RAB5 GTPases in stomatal immunity rather than defence in the apoplast⁵⁴.

We next addressed whether *rha1*, *ara7*, *ara6* and *ara6 x ara7* mutants are affected in other MAMP-induced defences, including activation of MAP kinases and the ROS burst required for stomatal closure⁵⁵. Overall, activation of MAP kinases induced by flg22 treatment were similar in all *rab5* GTPase mutants and wild type plants (Figure 3C). Likewise, flg22-induced ROS production was observed in all *rab5* GTPase mutants with *rha1*, *ara7* and *ara6* to a

similar extent as wild type plants and only *ara6 x ara7* mutants showing elevated ROS production (Figure 3D). These findings suggest that impaired stomatal closure to flg22 is not caused by general defects in flg22-induced signalling, and further imply that a lack of ROS production may not be the cause of the stomatal impairment. One explanation for the elevated ROS production observed in *ara6 x ara7* mutants could be due to impaired trafficking of RBOHD⁵⁶. Additionally, we found that the *rha1*, *ara7*, *ara6* and *ara6 x ara7* mutants were not generally immune-compromised as they supported similar levels of powdery mildew penetration (Figure S10), a fungal pathogen that does not infect plants through stomata^{17 52}.

RAB5 GTPases regulate FLS2 endocytosis

We have previously shown that ARA7 plays a critical role in endocytosis of flg22-activated FLS2 using overexpression of dominant-negative ARA7⁵⁷. To examine whether the *rab5* GTPase mutants were affected in FLS2 endocytosis, we generated homozygous crosses of Col-0/*FLS2p::FLS2-GFP* plants with *rha1*, *ara7*, *ara6* and *ara6 x ara7* mutants. Using high-throughput confocal imaging and quantitative image analysis by EndoQuant⁵⁷ we found that FLS2 endosomal numbers were elevated in *ara6* mutants at late time points compared to wild type plants (Figure 4A), similar to the effect by Wortmannin treatment⁵⁷. By contrast, *rha1* and *ara7* had significantly lower FLS2 endosomal numbers upon flg22 treatment (Figure 4B and C). Reduced flg22-induced FLS2 endosomal numbers in *ara7* and *rha1* mutants are consistent with inhibition of FLS2 endocytosis upon overexpression of dominant-negative ARA7⁵⁷. Together with the finding that ARA7 partially localizes with markers of the *trans*-Golgi network (TGN), it suggests that the conventional RAB5 GTPases ARA7 and RHA1 act in early stages of post-TGN trafficking, while ARA6 preferentially localizing to late endosomes^{46 47} seems to regulate later stages of FLS2 trafficking to the vacuole. Interestingly, *ara6 x ara7* mutants accumulated FLS2 endosomes at similar levels to wild type plants at most time points, with FLS2 endosomal numbers only reduced at early time points (Figure 4D). This is consistent with the hypothesis that activated FLS2 sequentially traffics along ARA7- and then ARA6-positive compartments⁵⁷. It is possible that *ara7* mutants reduced in FLS2 endosomes and *ara6* mutants accumulating more FLS2 endosomes (Figure 4A and B) level both effects.

Discussion

There are several examples where quantitative high-throughput imaging of cellular parameters has been used to probe the intersection between the endomembrane system and signal transduction events^{9 32 35}. The guard cell response is relatively well understood and involves the endomembrane system^{16 21 33 45}. The core guard cell pathway that results in a change in stomatal aperture could be divided into i) signal transduction and ii) translation of the signal into a biomechanical response. The closure of stomata is mediated by a decrease in guard cell volume, which is driven by the release of cytosolic K⁺ triggering water to move out¹⁶. This change in volume coincides with surface area changes of up to 40%^{33 58}. The most widely accepted hypothesis is that removal of membrane from the PM to the vacuole facilitates the change in surface area³³. Fusion and fission of vesicles have been observed during the swelling and shrinking of guard cells^{59 60 61}. The clathrin machinery regulates the removal of membranes in the form of vesicles, thereby contributing to coordinated membrane traffic⁶². Mutants in *CHC1* and in *SYP121/PEN1* are both affected in stomatal aperture control and in coordinated vesicle transport⁶³. Interestingly, *chc2* mutants were specifically impaired in flg22- but not ABA-induced stomatal closure³⁴. Disruption of the endomembrane system could differentially affect distinct guard cell signalling pathways leading to closure.

The identified genetic components of the endomembrane system that affect stomatal closure appear to intersect the guard cell response in three different categories: i) SCAMP1, SCAMP2, SCAMP4, SYP41, SYP121/PEN1, SYT1, VTI11 and REM1 appear to be involved in general stomatal closure as none of the five triggers could induce the closure of stomata in the respective mutants (Figure 2). Their identification highlights the intersection of the endomembrane system with the core guard cell signalling pathway leading to stomatal closure. ii) SYP21, VAMP721, VAMP722, VTI12, RABA1D, RABG3B and EPSIN1 represent membrane trafficking regulators, which seem to be predominantly required for stomatal closure induced by MAMPs and second messengers but not ABA. iii) SCAMP5-, ARA7- and ARA6-regulated membrane traffic seems to be critical for stomatal closure in

Accepted Article

response to two but dispensable to three of the five triggers. Given that each category appears to contain members of the same gene families such as the SCAMPs, it is possible that different members of gene families regulating membrane trafficking intersect with one or more guard cell signalling pathways. This would suggest that the endomembrane system intersects with guard cell signalling at different levels: i) signal perception of the individual trigger; ii) signal transduction including crosstalk between events triggered by several triggers; and iii) signal response, which results in the closure induced by all triggers. It would be interesting to investigate these relationships in future experiments.

In this study, we identified that *rha1*, *ara7*, *ara6* and *ara6 x ara7* were impaired in MAMP-induced stomatal closure but not generally non-responsive to flg22 or immune-compromised (Figure 2, Figure 3, Figure S10). The inability to close stomata in response to flg22 in these mutants is therefore affecting the intersection between the endomembrane system and guard cell signalling upstream of the core guard cell pathway. Like *chc2* and *vps37-1*^{34 35}, the *rab5* GTPase mutants were affected in FLS2 endocytic trafficking (Figure 5). Yet, *ara7* and *rha1* caused a reduction in FLS2 endosomal accumulation while *ara6* showed more accumulation of FLS2 endosomes, and the *ara6 x ara7* double mutant was only affected at early not late time points of FLS2 endocytosis (Figure 4). Thus, there is no obvious correlation between FLS2 endosomal accumulation and FLS2-mediated stomatal closure. In agreement, flg22-induced degradation of FLS2 was observed in all *rab5* GTPase mutants (Figure 4C). The apparent non-redundant function of the three RAB5 GTPases in flg22-induced stomatal closure is curious and future studies into the possibility of these GTPases functioning as a complex may prove interesting.

In summary, our quantitative high-throughput imaging screen resulted in a genetic framework of stomatal closure. This provides a starting point for the molecular dissection of guard cell signalling upstream and downstream of the core guard cell pathway and the intersection with the endomembrane system regulating stomatal closure. This approach revealed novel, non-redundant roles for RAB5 GTPases in stomatal immunity. This highlights that cell type-specific responses aid functional dissection of homologous genes, which when generating

higher order knock-out mutants causes pleiotropic effects up to lethality⁶⁴. In addition, timed quantitative high-throughput imaging further revealed roles of the three homologous RAB5 GTPases in FLS2 endocytic trafficking. Thus, high-throughput imaging at cellular and subcellular scales enables genetic dissection of plant physiological response to biotic and abiotic stresses.

Materials and Methods

Plant materials and growth conditions

Arabidopsis thaliana seeds were obtained from Nottingham *Arabidopsis* Seed Centre (NASC) and kindly provided by collaborators (Table S1). T-DNA insertions were checked by PCR using the appropriate primer pairs indicated in Table S1, and homozygous mutants were selected for further analysis. *ara6*, *ara7* and *rha1* mutants expressing FLS2-GFP were obtained by crossing them with the Col-0/*FLS2p::FLS2-3xmyc-GFP* line⁵⁷. F3 generations, which carried homozygous T-DNA insertions in the *RAB5 GTPase* genes and homozygous *FLS2p::FLS2-3xmyc-GFP* transgenes confirmed by PCR, were selected for further analysis. Plants were grown on general soil (*Arabidopsis* mix, John Innes Centre, Norwich) at 100 $\mu\text{mol m}^{-2} \text{s}^{-1}$ PFD and 12 or 16 hr days, 20 or 22°C, and 65% humidity.

Stomatal closure assays

Stomatal closure assays were optimized for each treatment. For flg22 and ABA treatments, cotyledons (one cotyledon from three plants per genotype) from 14-16 days old plants grown at 16 hrs/20°C were removed the night before and floated in buffer (5 mM KCl, 50 μM CaCl₂, 10 mM MES-TRIS, pH 6.15) in the same cabinet as they were grown. The following day, 2-3 hrs after lights had come on, the buffer was supplemented with 10 μM flg22 (EZBiolabs) or 5 μM ABA (Sigma-Aldrich) final concentrations, and cotyledons were incubated for 2 hrs (staggered application so that image acquisition was exactly 2 hrs after treatment). For treatments with chitin, H₂O₂ and CaCl₂, cotyledons from plants grown at 12 hrs/22°C were used, floated in buffer (10 mM MES, 50 mM KCl, pH 6.15), and treated with 1mg/ml chitin (Nacosy), 100 μM H₂O₂ (Sigma-Aldrich), or 10 mM CaCl₂ (Sigma-Aldrich).

High-throughput confocal microscopy

For imaging stomatal pores, cotyledons were transferred to 96-well plates with the lower epidermis facing the optical glass bottoms (Greiner), and high throughput confocal imaging was performed using the spinning disc automated Opera microscope (Perkin-Elmer Cellular Technologies) as described¹². Stomatal pores were imaged based on autofluorescence of the

guard cell lip (Figure 1). Excitation of the samples was performed at 405 nm and the emission captured using the 540/570 band-pass filter. The exposure time was set to 120 ms per image. Images of a consecutive series of 25 planes with a distance of 1 μm were taken with a 20x objective and displayed as a maximum projection using Acapella software (Perkin-Elmer Cellular Technologies). Image acquisition for a full plate takes approximately 40 min with an average of 30 stomata detected per cotyledon.

Imaging of FLS2-GFP endosomes was performed as described ⁵⁷. Briefly, cotyledons of two weeks-old Col-0, *rha1*, *ara7* and *ara6* plants expressing FLS2-GFP were treated with 10 μM flg22 for the indicated times, transferred to 96-well plates and imaged with the Opera microscope. Quantification of FLS2-GFP endosomal numbers was done using the EndoQuant tool (<https://sourceforge.net/projects/bioimage/files/EndoQuant/>).

Quantitative imaging of stomatal apertures (StomataMeasurer)

Images of stomatal pores acquired with the high throughput confocal microscope were analysed with the image processing software Acapella (version 2.0; Perkin-Elmer). We designed an algorithm that robustly detects stomatal pores and quantifies distances between stomata (density), stomatal pore width and length (StomataMeasurer; Figure 1 and Figure S1). The algorithm initially enhances contrast of multiple regions of an image based on Curvelets Coefficient Transform to clean minor noise ^{65 66}. Following this, a quality control process is used to locate invalid image regions (Regions with very low intensities or contrast values), and images comprising less than 25% valid regions are rejected. Next, global adaptive thresholding ^{67 68} is used to identify stomata as regions of interest (ROI). Threshold values were based on the intensity distribution of an image (75% of the computed Otsu value), and after establishing an optimum threshold, background pixels were removed if they were lower than the threshold value. The results are saved as image objects, together with features such as size, length, width and intensity/contrast calculated. Objects then are filtered according to their size, width and length, intensity, and contrast if these values locate outside of the defined range (e.g. 25th-95th percentiles, 1 standard deviation, SD, for low values and 2SDs for high values). In this way, unsuitable objects are removed and those remaining represent the

Accepted Article

detected stomatal pores. The image is then inverted so that the (previously dark) pixels inside the stomatal pores are assigned with high intensity values. Local adaptive thresholding⁶⁸ is applied to identify the high intensity areas within each pore and the results are again saved as objects (which this time represent the detected inner pores). Threshold values were determined over a single region (over 95% of the distribution of regional characteristics, 2 standard deviation, SDs). Each stoma is numbered, images are saved as png files, and measurements of stomatal densities, pore width and length are exported and saved in a csv file for further analysis. The Acapella version of StomataMeasurer, which allows batch processing of images, is available at <https://github.com/TeamMacLean/AcapellaStomataMeasurer>. A modified open source version implemented in Python that will detect stomata from any TIFF fluorescence image (Figure S1) and a user manual is available at <https://github.com/TeamMacLean/StomataMeasurer>.

Quantitative analysis of stomatal apertures

Statistics and data analysis were performed, and plots produced using scripts developed in R (v. 3.2.1; R Core Team, 2013). The scripts made use of the R packages *SDMtools*⁶⁹, *TeachingDemos*⁷⁰, *boot*⁷¹, *gplots*⁷², *gtools*⁷³, *RColorBrewer*⁷⁴, *clustsig*⁷⁵, *plotrix*⁷⁶, *dendextend*⁷⁷, and *babar*⁷⁸. The statistical analysis focused on the output parameters stomatal pore width, stomatal length and average nearest neighbour distance between stomata per image as proxy for stomatal density. Parameter data was aggregated from images across at least three experimental replicates for each mutant and at least two corresponding replicates for Col-0 (or alternative reference mutant with consistently significant closing behaviour under the given treatment). All measurements are listed in Table S2. For each parameter, kernel density estimation was used to infer a probability density function for each mutant under each experimental condition (using R's *density* function). Means values were then calculated from these probability distributions. Where a ratio of means was plotted, standard errors were calculated by accounting for the standard error in each mean and combining using error propagation. Here the standard error of each mean was calculated using the original data points.

Accepted Article

Significant stomatal closure was tested using two independent methods. Firstly, since determination of the p-value is a standard approach for evaluating statistical significance, p-values were calculated based on the null hypothesis that the two sets of data (under treatment and control conditions) are drawn from the same distribution; data was aggregated such that the difference in means could be calculated between 1000 pairs of bootstrap samples and a two-tailed p-value obtained by calculating the proportion of the resulting distribution that has a larger absolute value than the true difference in means. Due to the recent recognition of potential issues surrounding the calculation of p-values, we secondly also compute Bayes factors as a demonstrably robust alternative and compare the hypothesis $H1$ that the two data samples are drawn from the same normal distribution (and so have the same mean and standard deviation) to the hypothesis $H2$ that the two samples are drawn from different normal distributions; the *compareDistributions* function from the R package, *babar*⁷⁸ was used to compute the log (Bayes factor) and interpreted according to Jeffreys' scale. We required a p-value < 0.05 and Bayes factor < -2 , showing substantial evidence for hypothesis $H2$, to conclude significant closure. Using both measures (p-values, and Bayes factors) provides two alternative and standard ways of analysing data that, in this case, give consistent results.

Figure 2 provides indication of the level of significant impairment in closing. Here we considered a number of thresholds based on p-values and Bayes factors (p-values > 0.05 and 0.1 and Bayes factors > -2 , indicating insubstantial evidence for hypothesis $H2$, and > 2 , indicating substantial evidence for hypothesis $H1$) and scored based on how many of these thresholds were passed. The results were clustered using average-linkage hierarchical clustering with the metric of Euclidean distance and the plot produced using the *heatmap.2* function in the R package, *gplots*. Statistically significant clusters were determined using the *simprof* function from the package, *clustsig*. Here the null hypothesis that “there is no a priori group structure” was rejected for p-values < 0.05 . Further, R's *clusterboot* function was used to assess the stability of these clusters using bootstrapping and computation of Jaccard similarities. Here stable clusters had a Jaccard similarity value of at least 0.75.

ROS burst assays

ROS assays were performed as described ⁷⁹. Briefly, 16 leaf discs were excised per genotype of four weeks-old soil-grown plants and treated with 100 nM flg22. ROS was measured with a charge-coupled device camera fitted to a computer monitor (Photek Ltd., East Sussex) for 50 min.

Immunoblot analysis

For immunoblot analysis of FLS2 protein levels and MAPK activation, total proteins from eight seedlings per treatment were extracted in Laemmli buffer (17% glycerol, 25 mM TRIS base, 2 % SDS, 0.005 % Bromophenol blue) supplemented with 1% plant protease inhibitor cocktail (Sigma), 1 % DTT and 1 mM PMSF. After denaturation for 10 min at 75°C, proteins were separated on 10 % SDS-PAGE gels and transferred on PVDF membrane (Immobilon-P, Millipore) using the BioRad semi-dry transfer apparatus, following manufacturer's instructions. The anti-FLS2 (Eurogentec custom) (1:5000 dilution) and anti-p42p44 (Cell Signalling) (1:1000 dilution) primary antibodies followed by the secondary anti-rabbit antibody coupled to horseradish peroxidase (HRP) (1:10,000 dilution) (Sigma Aldrich) were used for FLS2 protein and MAPK activation detections, respectively. HRP was detected using ECL reagents (Pierce ECL substrate, Thermo Scientific) and a SRX-101A (Konica Minolta) film developer.

Bacterial and fungal infections

Bacterial infections were performed as described ⁸⁰. Briefly, *Pto* DC3000 cor⁻ bacteria were grown for two days on plates, then scratched off and transferred into a solution of 10 mM MgCl₂ with 0.04 % Silwet L-77 (Lehle Seeds, USA) until reaching an optical density of OD₆₀₀ = 0.3. Plants were surface sprayed with the bacterial suspension. Bacterial numbers were scored three days post infection. Fungal infections using *Golovinomyces orontii* and *Erysiphe pisi* powdery mildew strains were performed as described ^{81 82}.

Acknowledgements

We like to thank members of the Robatzek laboratory for fruitful discussions, Emily Seward for technical help, and many colleagues for sharing materials. This research was funded by the

European Research Council (S.R.), the Gatsby Charitable Foundation (S.R.), and the by the Biotechnology and Biological Sciences Research Council Institute Strategic Programme 'Biotic interactions for crop productivity' (BB/J004553/1) (S.R., R.M.).

References

1. Hao T, Wu D, Zhao L, Wang Q, Wang E, Sun J. The Genome-Scale Integrated Networks in Microorganisms. *Front Microbiol.* 2018;9:296. doi:10.3389/fmicb.2018.00296
2. Berens ML, Berry HM, Mine A, Argueso CT, Tsuda K. Evolution of Hormone Signaling Networks in Plant Defense. *Annu Rev Phytopathol.* 2017;55(1):401-425. doi:10.1146/annurev-phyto-080516-035544
3. Scheres B, van der Putten WH. The plant perceptron connects environment to development. *Nature.* 2017;543(7645):337-345. doi:10.1038/nature22010
4. St Johnston D. The art and design of genetic screens: *Drosophila melanogaster*. *Nat Rev Genet.* 2002;3(3):176-188. doi:10.1038/nrg751
5. Wu L, Luo P, Di D-W, et al. Forward genetic screen for auxin-deficient mutants by cytokinin. *Sci Rep.* 2015;5(1):11923. doi:10.1038/srep11923
6. van Wersch R, Li X, Zhang Y. Mighty Dwarfs: Arabidopsis Autoimmune Mutants and Their Usages in Genetic Dissection of Plant Immunity. *Front Plant Sci.* 2016;7:1717. doi:10.3389/fpls.2016.01717
7. Hauser F, Chen W, Deinlein U, et al. A Genomic-Scale Artificial MicroRNA Library as a Tool to Investigate the Functionally Redundant Gene Space in Arabidopsis. *Plant Cell.* 2013;25(8):2848-2863. doi:10.1105/tpc.113.112805
8. Xuan W, Murphy E, Beeckman T, Audenaert D, De Smet I. Synthetic molecules: helping to unravel plant signal transduction. *J Chem Biol.* 2013;6(2):43-50. doi:10.1007/s12154-013-0091-8
9. Collinet C, Stöter M, Bradshaw CR, et al. Systems survey of endocytosis by multiparametric image analysis. *Nature.* 2010;464(7286):243-249. doi:10.1038/nature08779

- Accepted Article
10. Chuprov–Netochin R, Neskorođov Y, Marusich E, et al. Novel small molecule modulators of plant growth and development identified by high-content screening with plant pollen. *BMC Plant Biol.* 2016;16(1):192. doi:10.1186/s12870-016-0875-4
 11. Vasseur F, Bresson J, Wang G, Schwab R, Weigel D. Image-based methods for phenotyping growth dynamics and fitness components in *Arabidopsis thaliana*. *Plant Methods.* 2018;14(1):63. doi:10.1186/s13007-018-0331-6
 12. Salomon S, Grunewald D, Stüber K, et al. High-throughput confocal imaging of intact live tissue enables quantification of membrane trafficking in *Arabidopsis*. *Plant Physiol.* 2010;154(3). doi:10.1104/pp.110.160325
 13. Qi J, Wang J, Gong Z, Zhou J-M. Apoplastic ROS signaling in plant immunity. *Curr Opin Plant Biol.* 2017;38:92-100. doi:10.1016/j.pbi.2017.04.022
 14. Wang Y, Holroyd G, Hetherington AM, Ng CK-Y. Seeing “cool” and “hot”--infrared thermography as a tool for non-invasive, high-throughput screening of *Arabidopsis* guard cell signalling mutants. *J Exp Bot.* 2004;55(400):1187-1193. doi:10.1093/jxb/erh135
 15. Toda Y, Toh S, Bourdais G, Robatzek S, Maclean D, Kinoshita T. DeepStomata: Facial Recognition Technology for Automated Stomatal Aperture Measurement. *bioRxiv.* July 2018:365098. doi:10.1101/365098
 16. McLachlan DH, Kopischke M, Robatzek S. Gate control: guard cell regulation by microbial stress. *New Phytol.* 2014;203(4):1049-1063. doi:10.1111/nph.12916
 17. Faulkner C, Robatzek S. Plants and pathogens: Putting infection strategies and defence mechanisms on the map. *Curr Opin Plant Biol.* 2012;15(6). doi:10.1016/j.pbi.2012.08.009
 18. LEONARD KJ, SZABO LJ. Stem rust of small grains and grasses caused by *Puccinia graminis*. *Mol Plant Pathol.* 2005;6(2):99-111. doi:10.1111/j.1364-3703.2005.00273.x
 19. Melotto M, Underwood W, Koczan J, Nomura K, He SY. Plant Stomata Function in Innate Immunity against Bacterial Invasion. *Cell.* 2006;126(5):969-980. doi:10.1016/j.cell.2006.06.054
 20. Couto D, Zipfel C. Regulation of pattern recognition receptor signalling in plants. *Nat Rev Immunol.* 2016;16(9):537-552. doi:10.1038/nri.2016.77

21. Kim T-H, Böhmer M, Hu H, Nishimura N, Schroeder JI. Guard Cell Signal Transduction Network: Advances in Understanding Abscisic Acid, CO₂, and Ca²⁺ Signaling. *Annu Rev Plant Biol.* 2010;61(1):561-591. doi:10.1146/annurev-arplant-042809-112226
22. Negi J, Hashimoto-Sugimoto M, Kusumi K, Iba K. New Approaches to the Biology of Stomatal Guard Cells. *Plant Cell Physiol.* 2014;55(2):241-250. doi:10.1093/pcp/pct145
23. Hedrich R, Geiger D. Biology of SLAC1-type anion channels - from nutrient uptake to stomatal closure. *New Phytol.* 2017;216(1):46-61. doi:10.1111/nph.14685
24. Geiger D, Scherzer S, Mumm P, et al. Activity of guard cell anion channel SLAC1 is controlled by drought-stress signaling kinase-phosphatase pair. *Proc Natl Acad Sci U S A.* 2009;106(50):21425-21430. doi:10.1073/pnas.0912021106
25. Geiger D, Scherzer S, Mumm P, et al. Guard cell anion channel SLAC1 is regulated by CDPK protein kinases with distinct Ca²⁺ affinities. *Proc Natl Acad Sci U S A.* 2010;107(17):8023-8028. doi:10.1073/pnas.0912030107
26. Scherzer S, Maierhofer T, Al-Rasheid KAS, Geiger D, Hedrich R. Multiple calcium-dependent kinases modulate ABA-activated guard cell anion channels. *Mol Plant.* 2012;5(6):1409-1412. doi:10.1093/mp/sss084
27. Brandt B, Brodsky DE, Xue S, et al. Reconstitution of abscisic acid activation of SLAC1 anion channel by CPK6 and OST1 kinases and branched ABI1 PP2C phosphatase action. *Proc Natl Acad Sci U S A.* 2012;109(26):10593-10598. doi:10.1073/pnas.1116590109
28. Maierhofer T, Diekmann M, Offenborn JN, et al. Site- and kinase-specific phosphorylation-mediated activation of SLAC1, a guard cell anion channel stimulated by abscisic acid. *Sci Signal.* 2014;7(342):ra86. doi:10.1126/scisignal.2005703
29. Geiger D, Maierhofer T, Al-Rasheid KAS, et al. Stomatal Closure by Fast Abscisic Acid Signaling Is Mediated by the Guard Cell Anion Channel SLAH3 and the Receptor RCAR1. *Sci Signal.* 2011;4(173):ra32-ra32. doi:10.1126/scisignal.2001346
30. Guzel Deger A, Scherzer S, Nuhkat M, et al. Guard cell SLAC1-type anion channels mediate flagellin-induced stomatal closure. *New Phytol.* 2015;208(1):162-173. doi:10.1111/nph.13435

- Accepted Article
31. Montillet J-L, Leonhardt N, Mondy S, et al. An abscisic acid-independent oxylipin pathway controls stomatal closure and immune defense in Arabidopsis. Dangi JL, ed. *PLoS Biol.* 2013;11(3):e1001513. doi:10.1371/journal.pbio.1001513
 32. Surpin M, Raikhel N. Correction: Traffic jams affect plant development and signal transduction. *Nat Rev Mol Cell Biol.* 2004;5(2):100-109. doi:10.1038/nrm1311
 33. Meckel T, Gall L, Semrau S, Homann U, Thiel G. Guard cells elongate: relationship of volume and surface area during stomatal movement. *Biophys J.* 2007;92(3):1072-1080. doi:10.1529/biophysj.106.092734
 34. Mbengue M, Bourdais G, Gervasi F, et al. Clathrin-dependent endocytosis is required for immunity mediated by pattern recognition receptor kinases. *Proc Natl Acad Sci U S A.* 2016;113(39). doi:10.1073/pnas.1606004113
 35. Spallek T, Beck M, Ben Khaled S, et al. ESCRT-I Mediates FLS2 Endosomal Sorting and Plant Immunity. *PLoS Genet.* 2013;9(12). doi:10.1371/journal.pgen.1004035
 36. Faulkner C, Zhou J, Evrard A, et al. An automated quantitative image analysis tool for the identification of microtubule patterns in plants. *Traffic.* 2017;18(10):683-693. doi:10.1111/tra.12505
 37. Uemura T, Ueda T. Plant vacuolar trafficking driven by RAB and SNARE proteins. *Curr Opin Plant Biol.* 2014;22:116-121. doi:10.1016/j.pbi.2014.10.002
 38. Jayakody H, Liu S, Whitty M, Petrie P. Microscope image based fully automated stomata detection and pore measurement method for grapevines. *Plant Methods.* 2017;13(1):94. doi:10.1186/s13007-017-0244-9
 39. Yang M, Sack FD. The too many mouths and four lips mutations affect stomatal production in Arabidopsis. *Plant Cell.* 1995;7(12):2227-2239. doi:10.1105/tpc.7.12.2227
 40. Berger D, Altmann T. A subtilisin-like serine protease involved in the regulation of stomatal density and distribution in Arabidopsis thaliana. *Genes Dev.* 2000;14(9):1119-1131.
 41. Latz A, Becker D, Hekman M, et al. TPK1, a Ca²⁺-regulated Arabidopsis vacuole two-pore K⁺ channel is activated by 14-3-3 proteins. *Plant J.* 2007;52(3):449-459. doi:10.1111/j.1365-313X.2007.03255.x

- Accepted Article
42. Gudesblat GE, Iusem ND, Morris PC. Arabidopsis MPK3, a Key Signalling Intermediate in Stomatal Function. *Plant Signal Behav.* 2007;2(4):271-272.
 43. Hōrak H, Sierla M, Töldsepp K, et al. A Dominant Mutation in the HT1 Kinase Uncovers Roles of MAP Kinases and GHR1 in CO₂-Induced Stomatal Closure. *Plant Cell.* 2016;28(10):2493-2509. doi:10.1105/tpc.16.00131
 44. Sanderfoot AA, Raikhel N V. The specificity of vesicle trafficking: coat proteins and SNAREs. *Plant Cell.* 1999;11(4):629-642.
<http://www.ncbi.nlm.nih.gov/pubmed/10213783>. Accessed August 20, 2018.
 45. Eisenach C, Chen Z-H, Grefen C, Blatt MR. The trafficking protein SYP121 of Arabidopsis connects programmed stomatal closure and K⁺ channel activity with vegetative growth. *Plant J.* 2012;69(2):241-251. doi:10.1111/j.1365-313X.2011.04786.x
 46. Ueda T, Yamaguchi M, Uchimiya H, Nakano A. Ara6, a plant-unique novel type Rab GTPase, functions in the endocytic pathway of Arabidopsis thaliana. *EMBO J.* 2001;20(17):4730-4741. doi:10.1093/emboj/20.17.4730
 47. Ueda T, Uemura T, Sato MH, Nakano A. Functional differentiation of endosomes in Arabidopsis cells. *Plant J.* 2004;40(5):783-789. doi:10.1111/j.1365-313X.2004.02249.x
 48. Heard W, SklenáYJ, Tomé DFA, Robatzek S, Jones AME. Identification of Regulatory and Cargo Proteins of Endosomal and Secretory Pathways in Arabidopsis thaliana by Proteomic Dissection. *Mol Cell Proteomics.* 2015;14(7):1796-1813.
doi:10.1074/mcp.M115.050286
 49. Terryn N, Arias MB, Engler G, et al. rha1, a gene encoding a small GTP binding protein from Arabidopsis, is expressed primarily in developing guard cells. *Plant Cell.* 1993;5(12):1761-1769. doi:10.1105/tpc.5.12.1761
 50. Shang Y, Dai C, Lee MM, Kwak JM, Nam KH. BRI1-Associated Receptor Kinase 1 Regulates Guard Cell ABA Signaling Mediated by Open Stomata 1 in Arabidopsis. *Mol Plant.* 2016;9(3):447-460. doi:10.1016/j.molp.2015.12.014
 51. Kong L, Cheng J, Zhu Y, et al. Degradation of the ABA co-receptor ABI1 by PUB12/13 U-box E3 ligases. *Nat Commun.* 2015;6(1):8630. doi:10.1038/ncomms9630

- Accepted Article
52. Koers S, Guzel-Deger A, Marten I, Roelfsema MRG. Barley mildew and its elicitor chitosan promote closed stomata by stimulating guard-cell S-type anion channels. *Plant J.* 2011;68(4):670-680. doi:10.1111/j.1365-313X.2011.04719.x
 53. Shinya T, Yamaguchi K, Desaki Y, et al. Selective regulation of the chitin-induced defense response by the Arabidopsis receptor-like cytoplasmic kinase PBL27. *Plant J.* 2014;79(1):56-66. doi:10.1111/tpj.12535
 54. Zeng W, Brutus A, Kremer JM, et al. A Genetic Screen Reveals Arabidopsis Stomatal and/or Apoplastic Defenses against *Pseudomonas syringae* pv. tomato DC3000. Rathjen J, ed. *PLoS Pathog.* 2011;7(10):e1002291. doi:10.1371/journal.ppat.1002291
 55. Kadota Y, Sklenar J, Derbyshire P, et al. Direct Regulation of the NADPH Oxidase RBOHD by the PRR-Associated Kinase BIK1 during Plant Immunity. *Mol Cell.* 2014;54(1):43-55. doi:10.1016/j.molcel.2014.02.021
 56. Hao H, Fan L, Chen T, et al. Clathrin and Membrane Microdomains Cooperatively Regulate RbohD Dynamics and Activity in Arabidopsis. *Plant Cell.* 2014;26(4):1729-1745. doi:10.1105/tpc.113.122358
 57. Beck M, Zhou J, Faulkner C, Mac D, Robatzek S. Spatio-temporal cellular dynamics of the Arabidopsis flagellin receptor reveal activation status-dependent endosomal sorting. *Plant Cell.* 2012;24(10). doi:10.1105/tpc.112.100263
 58. Shope JC, DeWald DB, Mott KA. Changes in surface area of intact guard cells are correlated with membrane internalization. *Plant Physiol.* 2003;133(3):1314-1321. doi:10.1104/pp.103.027698
 59. Homann U, Thiel G. Unitary exocytotic and endocytotic events in guard-cell protoplasts during osmotically driven volume changes. *FEBS Lett.* 1999;460(3):495-499. <http://www.ncbi.nlm.nih.gov/pubmed/10556524>. Accessed August 20, 2018.
 60. Homann U, Thiel G. The number of K⁺ channels in the plasma membrane of guard cell protoplasts changes in parallel with the surface area. *Proc Natl Acad Sci.* 2002;99(15):10215-10220. doi:10.1073/pnas.152324399
 61. Meckel T, Hurst AC, Thiel G, Homann U. Endocytosis against high turgor: intact guard cells of *Vicia faba* constitutively endocytose fluorescently labelled plasma membrane and GFP-tagged K⁺-channel KAT1. *Plant J.* 2004;39(2):182-193.

doi:10.1111/j.1365-313X.2004.02119.x

62. Baisa GA, Mayers JR, Bednarek SY. Budding and braking news about clathrin-mediated endocytosis. *Curr Opin Plant Biol.* 2013;16(6):718-725.
doi:10.1016/j.pbi.2013.09.005
63. Larson ER, Van Zelm E, Roux C, Marion-Poll A, Blatt MR. Clathrin Heavy Chain Subunits Coordinate Endo- and Exocytic Traffic and Affect Stomatal Movement. *Plant Physiol.* 2017;175(2):708-720. doi:10.1104/pp.17.00970
64. Dainobu, T., Saito, C., Ueda, T. and Nakano A. Functional analysis of RHA1 and ARA7 in Arabidopsis pollen development and function. In: *Abstract of the Annual Meeting of JSPP.* ; 2009:doi:10.14841/jspp.2009.0.0332.0.
65. Starck, J.L., Murtagh, F., Candès, E.J. and Donoho DL. Gray and color image contrast enhancement by the curvelet transform. *IEEE Trans Image Process.* 2003;12:706-717.
66. Russ J. Seeing the scientific image (parts1,2,3). *Proc Roy Microsc Soc.* 2004;39(2, 3, 4):(2), 1-18; (3), 1-15; (4), 1-15.
67. Otsu N. A threshold selection method from gray-level histograms. *IEEE Trans Syst Man Cybern.* 1979;1(9):62-66. doi:10.1109/TSMC.1979.4310076
68. Sezgin, M. and Sankur B. Survey over image thresholding techniques and quantitative performance evaluation. *J Electron Imaging.* 2004;13:146–165.
69. Van Der Wal, J., L. Falconi, S. Januchowski, L. Shoo, Storlie. C. SDMTTools: species distribution modelling tools: tools for processing data associated with species distribution modelling exercises. <http://CRAN.R-project.org/package=SDMTTools>.
70. Snow G. TeachingDemos: Demonstrations for Teaching and Learning. <https://cran.r-project.org/package=TeachingDemos>.
71. Canty, A. and Ripley B. Boot: Bootstrap Functions. <https://cran.r-project.org/package=boot>.
72. Warnes, R.G., Bolker, B., Bonebakker, L., Gentleman, R. et al. gplots: Various R Programming Tools for Plotting Data. <https://cran.r-project.org/package=gplots>.
73. Warnes, R.G., Bolker, B. and Lumley T. gtools: Various R Programming Tools. <https://cran.r-project.org/package=gtools>.
74. Neuwirth E. RColorBrewer: ColorBrewer Palettes. <https://cran.r->

project.org/package=RColorBrewer.

75. Suzuki, R. and Shimodaira H. Hierarchical Clustering with P-Values via Multiscale Bootstrap Resampling. <http://www.sigmath.es.osaka-u.ac.jp/shimo-lab/prog/pvclust/>.
76. Lemon J. Plotrix: a package in the red light district of R. *R-News*. 2006;6:8-12.
77. Galili T. dendextend: an R package for visualizing, adjusting, and comparing trees of hierarchical clustering. *Bioinformatics*. 2015;(doi: 10.1093/bioinformatics/btv428).
78. Rickett LM, Pullen N, Hartley M, et al. Incorporating prior knowledge improves detection of differences in bacterial growth rate. *BMC Syst Biol*. 2015;9(1):60. doi:10.1186/s12918-015-0204-9
79. Roux M, Schwessinger B, Albrecht C, et al. The Arabidopsis leucine-rich repeat receptor-like kinases BAK1/SERK3 and BKK1/SERK4 are required for innate immunity to hemibiotrophic and biotrophic pathogens. *Plant Cell*. 2011;23(6):2440-2455. doi:10.1105/tpc.111.084301
80. Zipfel C, Robatzek S, Navarro L, et al. Bacterial disease resistance in Arabidopsis through flagellin perception. *Nature*. 2004;428(6984). doi:10.1038/nature02485
81. Consonni C, Humphry ME, Hartmann HA, et al. Conserved requirement for a plant host cell protein in powdery mildew pathogenesis. *Nat Genet*. 2006;38(6):716-720. doi:10.1038/ng1806
82. Consonni C, Bednarek P, Humphry M, et al. Tryptophan-Derived Metabolites Are Required for Antifungal Defense in the Arabidopsis mlo2 Mutant. *PLANT Physiol*. 2010;152(3):1544-1561. doi:10.1104/pp.109.147660

Figure Legends

Figure 1. Image processing for the extraction of stomatal pores using StomataMeasurer.

(A) An autofluorescence stomata pore image with high background noise acquired by the Opera confocal microscope. (B) Image filters are applied to clean noise and enhance high contrast areas. A quality control process is used to scan the resulting image for invalid image areas (regions of very low intensity or contrast, shown in red) and images with less than 25% validity are rejected. (C) A global adaptive thresholding method identifies regions of interest and the results are saved as image objects (randomly coloured). (D) Filtering methods are employed to remove unsuitable objects according to their size, width and length, intensity, and contrast. Holes within the remaining object bodies are computationally filled and new image objects (red) are created, which represent the stomata pores. (E) The image is inverted, therefore highlighting the stomata inner apertures within each pore (enclosed by red lines). (F) A local adaptive thresholding method detects the high-intensity pixels within every pore and the results are saved as stomata inner aperture objects (red). (G-H) Stomata pore objects (randomly coloured in G) are overlapped with their corresponding inner aperture objects (green in H) and morphological traits are measured. (I) Quantification results for every detected pore (labelled) are saved in a CSV file for further analysis. (J-K) Representation of stomatal width and means (dashed lines) used for data analysis. Scale bar = 50 μm .

Figure 2. Integrated cluster analysis of stomatal closing compares phenotypes across all treatments.

Closing behaviour is illustrated for each mutant in response to flg22, chitin, ABA, CaCl_2 and H_2O_2 treatments. Colour coding: Green indicates closure in response to a treatment whilst purple and orange indicate statistically significant less closure and opening, respectively, compared to the reference measurements. The intensity of purple is proportional to a scale of scoring depending on the combined results of a Student's t-test ($p < 0.05$ and $p < 0.1$ to score lack of closing) and Bayesian statistical testing. Grey indicates a treatment that was not tested. Mutants are clustered according to similarity in stomatal behaviours across treatments. Eight clusters strongly supported by the data ($p < 0.05$) are indicated with red rectangles and numbers.

Figure 3. RAB5 GTPases RHA1, ARA7 and ARA6 mediate stomatal immunity. *RAB5* GTPase mutants show enhanced susceptibility to *Pto* DC3000 cor- (A) compared to Col-0, 3 days after spray infection but not after leaf injection (B). Bars represent the mean +/- SE (n = 8). Experiments have been repeated independently at least two times with similar results. Asterisks indicate a statistically significant difference compared to Col-0 WT, according to a Student's t-test ($p < 0.05$). (C) Immunoblot analysis of MAP kinase activation of Col-0 and the indicated *rab5* GTPase mutants measured in two weeks-old seedlings treated with flg22 for the indicated time points. (D) Total ROS burst of Col-0 and the indicated *rab5* GTPase mutants measured as relative light units (RLU) in leaf disks of 4 weeks-old plants treated with flg22.

Figure 4. RAB5 GTPase mutants differentially affect FLS2 endosomal accumulation. Measurement of FLS2-GFP endosomal numbers in cotyledons of Col-0 and the indicated *rab5* GTPase mutants of two weeks-old seedlings following treatment with 10 μ M flg22 for the indicated time points. Bars represent mean values +/- SD; average image number = 60 images from three independent experiments for *rha1* and *ara6 x ara7* and six independent experiments for *ara7* and *ara6*, with an average number of 100 images. Asterisks indicate a statistically significant difference compared to Col-0 at the same time point according to a Student's t-test (* = $p < 0.05$; ** = $p < 0.01$; *** = $p < 0.001$).

Supplemental Information

Supplemental Figure 1. Comparison of stomatal pore analysis. (A-B) Acapella StomataMeasurer and manual measurements. Using over 100 measurements obtained by screening Col-0 plants under control and treatment conditions, stomatal morphological parameters were extracted using both the algorithm and manual methods. Bar-charts show the mean and standard deviation of parameters and probability density curves show the entire distribution of values. The algorithm consistently overestimates stomatal width and also has a slightly larger variance. However, the qualitative closing behaviour is conserved between the two methods (difference in means between treatments 0.52 μm under manual measurement versus 0.46 μm for the algorithm and significant closing observed in both cases; testing using either a Student's t-test ($p < 0.05$) or Bayes factors. **(C-D)** Acapella StomataMeasurer and open source StomataMeasurer. Using data from three experiments screening *syp122* plants under control and treatment conditions, stomatal morphological parameters were extracted using both the Acapella and open source Python algorithms. Bar-charts show the mean and standard deviation of parameters and probability density curves show the entire distribution of values. The open source method is less sensitive than the Acapella method as it lacks an ellipse closing algorithm, available through Perkin Elmer, which allows for the successful detection of a larger number of pores. However, planned future fine-tuning of image analysis parameters will improve the successful detection rate of the open source algorithm. Nevertheless, the qualitative closing behaviour is conserved between the two methods and significant closing observed in both cases; testing using a Student's t-test ($p < 0.05$).

Supplemental Figure 2. Quantitative imaging of stomata identifies stomatal development patterns. (A) Stomatal patterns were quantified for each mutant (black dots) and compared to Col-0 data taken across all experiments (blue dot). For each parameter (stomatal length or nearest neighbour distance between stomata) a probability distribution was inferred from the combined data over all experiments, from which the mean value was calculated. Numbers correspond to mutant labelling in Supplemental Table S1. Three mutants with significant

developmental defects in stomatal patterning can be observed, 48 = *sddl-1*, 57 = *tmm* and 58 = *tpk1*. For four of the significant mutant clusters mentioned in the text as arising from Figure 5, the mean stomatal length is further plotted against stomatal closure after 2 hrs treatment with (B) 10 μ M flg22 and (C) 5 μ M ABA.

Supplemental Figure 3. (A) Stomatal closure to 0.1, 1 or 10 μ M of flg22 or ABA treatment is dose dependent. Bars represent mean values \pm SE; n = 150. **(B)** Stomatal closure kinetic is not perturbed in the OPERA microscope. Stomatal closure upon flg22 and ABA treatment follow the same course, and reaches a maximum after 60 min of treatment. Untreated stomata remain open after 60 min of image acquisition. The data represent the stomatal aperture of a population of 50 stomata of 2 independent experiments. The same population of stomata has been imaged during 1 hr every 10 min in untreated conditions, after ABA and flg22 treatments. Error bars represent mean values \pm SE; n = 60. A and B $\ast = p < 0.05$ following a Student t-test comparison of treatment vs control.

Supplemental Figure 4. Quantitative imaging of stomata identifies impaired flg22 closure patterns. Quantification of closure after 2 hrs treatment with 10 μ M flg22 across genotypes. Bar plots show **(A)** the ratio of mean stomatal pore width upon treatment over mean width under control conditions, and **(B)** the mean width under control conditions. Error bars represent the standard errors. Numbers in brackets correspond to mutant labelling in Supplemental Table S1. Asterisks indicate mutants with significant closing behaviour according to the results of statistical testing, where closing is tested using both a Student's t-test ($p < 0.05$ for significant closing) and Bayes factors (< -2 for significant closing). The number of data points used for the calculation of each mean making up the ratio is indicated next to each bar plot.

Supplemental Figure 5. Quantitative imaging of stomata identifies impaired ABA closure patterns. Quantification of closure after 2 hrs treatment with 5 μ M ABA across genotypes. Bar plots show **(A)** the ratio of mean stomatal pore width upon treatment over mean width under control conditions, and **(B)** the mean width under control conditions. Error

Accepted Article

bars represent the standard errors. Numbers in brackets correspond to mutant labelling in Supplemental Table S1. Asterisks indicate mutants with significant closing behaviour according to the results of statistical testing, where closing is tested using both a Student's t-test ($p < 0.05$ for significant closing) and Bayes factors (< -2 for significant closing). The number of data points used for the calculation of each mean making up the ratio is indicated next to each bar plot.

Supplemental Figure 6. Quantitative imaging of stomata identifies impaired chitin closure patterns. Quantification of closure after 2 hrs treatment with 1mg/ml chitin across genotypes. Bar plots show **(A)** the ratio of mean stomatal pore width upon treatment over mean width under control conditions, and **(B)** the mean width under control conditions. Error bars represent the standard errors. Numbers in brackets correspond to mutant labelling in Supplemental Table S1. Asterisks indicate mutants with significant closing behaviour according to the results of statistical testing, where closing is tested using both a Student's t-test ($p < 0.05$ for significant closing) and Bayes factors (< -2 for significant closing). The number of data points used for the calculation of each mean making up the ratio is indicated next to each bar plot.

Supplemental Figure 7. Quantitative imaging of stomata identifies impaired closure patterns by second messengers. Quantification of closure after 2 hrs treatment with 10 mM CaCl_2 across genotypes. Bar plots show **(A)** the ratio of mean stomatal pore width upon treatment over mean width under control conditions, and **(B)** the mean width under control conditions. Error bars represent the standard errors. Numbers in brackets correspond to mutant labelling in Supplemental Table S1. Asterisks indicate mutants with significant closing behaviour according to the results of statistical testing, where closing is tested using both a Student's t-test ($p < 0.05$ for significant closing) and Bayes factors (< -2 for significant closing). The number of data points used for the calculation of each mean making up the ratio is indicated next to each bar plot.

Supplemental Figure 8. Quantitative imaging of stomata identifies impaired closure

patterns by second messengers. Quantification of closure after 2 hrs treatment with 100 μ M H₂O₂ across genotypes. Bar plots show **(A)** the ratio of mean stomatal pore width upon treatment over mean width under control conditions, and **(B)** the mean width under control conditions. Error bars represent the standard errors. Numbers in brackets correspond to mutant labelling in Supplemental Table S1. Asterisks indicate mutants with significant closing behaviour according to the results of statistical testing, where closing is tested using both a Student's t-test ($p < 0.05$ for significant closing) and Bayes factors (< -2 for significant closing). The number of data points used for the calculation of each mean making up the ratio is indicated next to each bar plot.

Supplemental Figure 9. Multi-parametric quantitative imaging of stomata confirms mutants generally impaired in closure are not impaired in stomatal development.

Quantification of Ca²⁺- and ROS-induced stomatal immunity across those genotypes impaired in closure for all treatments. The graph compares mean stomatal length to the mean width change based on inferred probability distributions for each parameter. Numbers correspond to mutant labelling in Supplemental Table S1. The blue dot illustrates a representative Col-0 mean width change plotted against the mean Col-0 stomatal length using data taken across all experiments. The mutants, 48 = *sdd1-1* and 57 = *tmm* are added for comparison, to show typical mean lengths for mutants that are developmentally impaired.

Supplemental Figure 10. RAB5 GTPase mutants *rha1*, *ara7* and *ara6* are not general immune-compromised.

5-week-old plants of the indicated genotypes were inoculated with virulent *G. orontii* (A) or avirulent *E. pisi* (B) and % host cell entry was determined at 48 hpi (A) or 6 dpi (B), respectively. Data represent means of 3 independent biological replicates +/- SE. Distinct lower-case letters indicate statistically significant differences between groups as determined by One-way ANOVA and Tukey's post hoc test ($P \leq 0.05$). Each independent biological replicate comprised 4 plants and 4 leaves/plant, respectively. A minimum of 100 penetration events/plant were evaluated.

Supplemental Table S1. List of mutants used in this study.

Supplemental Table S2. List of all stomatal measurements.

Accepted Article

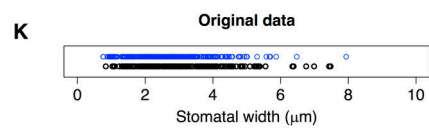
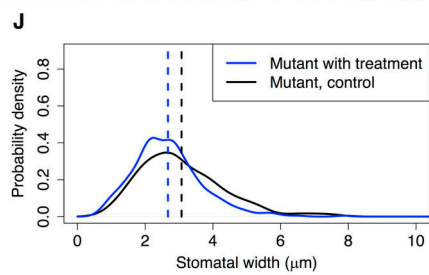
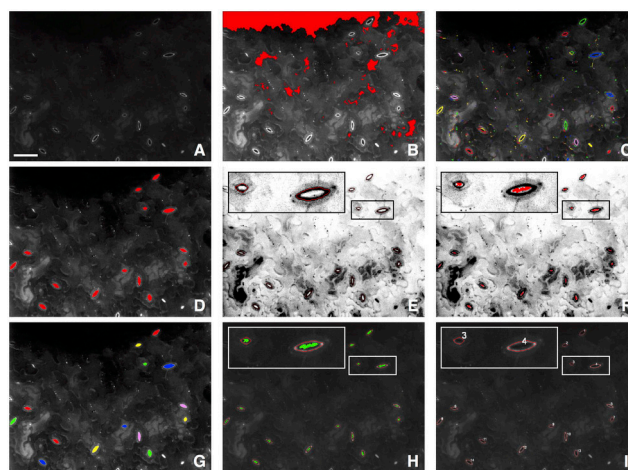


Figure 1.jpg

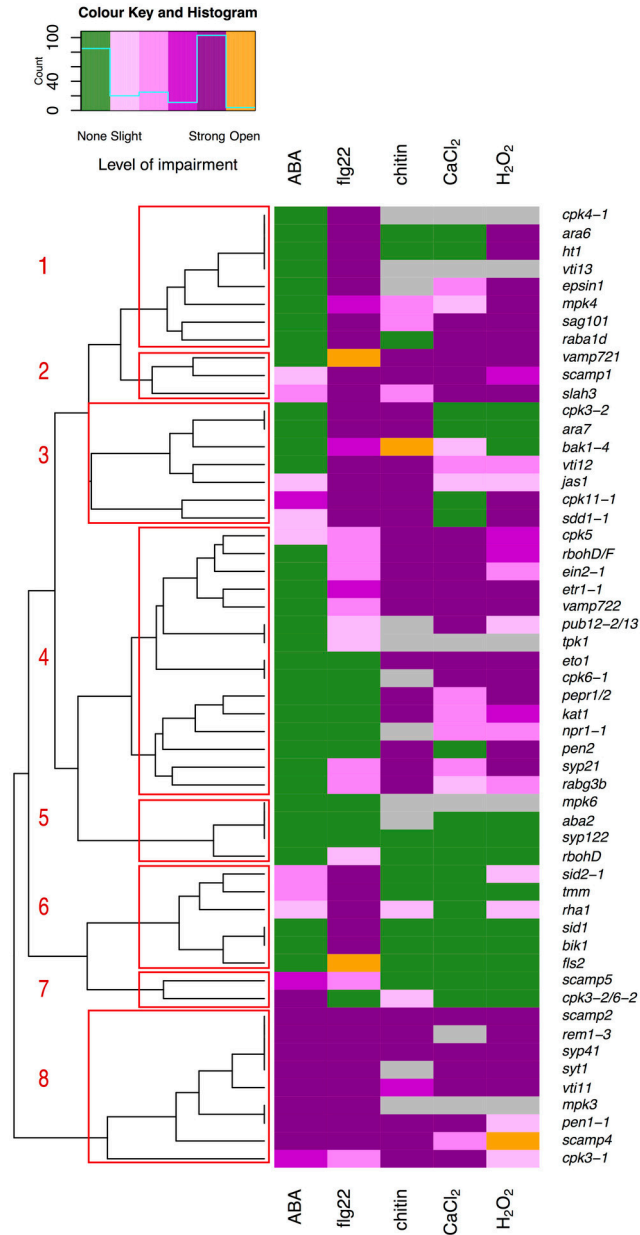


Figure 2.jpg

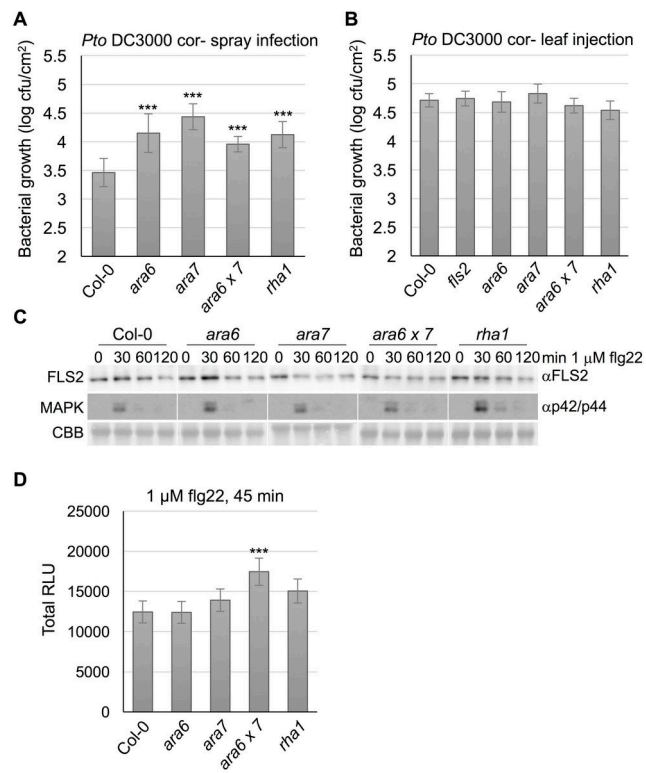


Figure 3.jpg

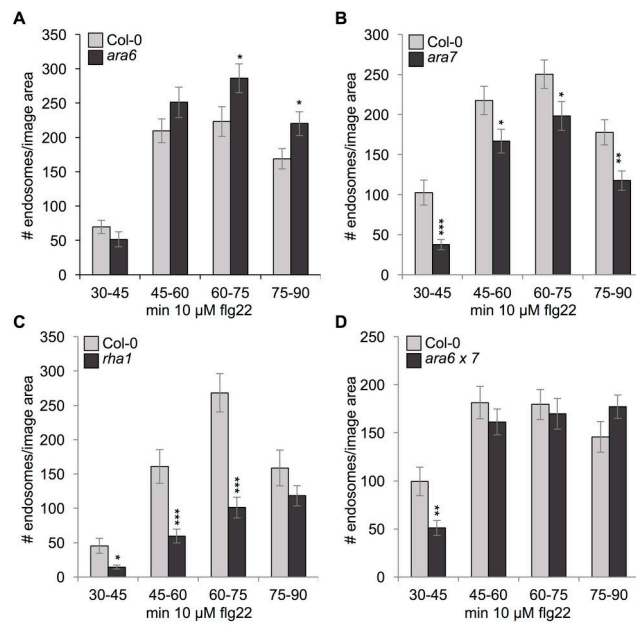


Figure 4.jpg